ORIGINAL PAPER

Rubus ellipticus fruits extract-mediated cuprous oxide nanoparticles: in vitro antioxidant, antimicrobial, and toxicity study

Jyoti Dhatwalia[1] · Amita Kumari[1] · Ankush Chauhan[2] · Khalid Mujasam Batoo[3] · Antara Banerjee[2] ·
Arunkumar Radhakrishnan[4] · Shabnam Thakur[1] · Ishita Guleria[1] · Sohan Lal[1] · Suresh Ghotekar[5] ·
Byung Hyune Choi[6] · Rajesh Kumar[7]

Abstract

The aim of the present study was to synthesize biologically active cuprous oxide nanoparticles (Cu_2O-NPs) using green nanotechnology from aqueous extract of *Rubus ellipticus* fruits. The structural characterization of aqueous extract-mediated cuprous oxide nanoparticles (Ru-Cu_2O-NPs) was performed using X-ray powder diffraction (XRD), Transmission electron microscope (TEM), Field emission scanning electron microscope (FE-SEM), Fourier-transform infrared spectroscopy (FTIR), X-ray photoelectron spectroscopy (XPS), and UV–Vis spectroscopy. Using standard techniques, Ru-Cu_2O-NPs were also evaluated for their biological activities (antioxidant, antimicrobial, and anticancer) and toxicity. The XRD patterns and Rietveld refinement confirmed the phase purity of Ru-Cu_2O-NPs with an average crystallite size of 25 nm. The FE-SEM and TEM images showed the formation of octahedron cages with a grain size of 0.82 ± 0.04 μm on average. The XPS analysis confirmed the presence of Cu^{1+} ions with many chemisorbed species on the surface. The determination of functional groups was carried out using FTIR with Cu–O stretching vibration at 635 cm^{-1}. Tauc's plot determined that the optical bandgap of the synthesized Ru-Cu_2O-NPs was 1.28 eV. Compared to aqueous fruit extract, Ru-Cu_2O-NPs showed significantly lower antioxidant activity. Furthermore, they showed higher antimicrobial activity (MIC) against *Bacillus subtilis* and *Rosellinia necatrix* (7.81 μg/mL), *Staphylococcus aureus* (15.62 μg/mL), and *Escherichia coli, Pseudomonas aeruginosa,* and *Fusarium oxysporum* (31.2 μg/mL). The Ru-Cu_2O-NPs showed no toxicity against BM MSCs and HC cells at 12.5 μg/mL concentration, whereas the Ru-Cu_2O-NPs showed anticancer activity against colon cancer cell lines (SW480 and SW620) at 100 g/mL concentration. These results indicate that Ru-Cu_2O-NPs have good antimicrobial and anticancer properties but have low toxicity thus making them suitable for use in pharmaceuticals and food industries.

Keywords *R. ellipticus* · Nanoparticles · Antioxidant · Antimicrobial · Toxicity

✉ Amita Kumari
amitabot@gmail.com

✉ Ankush Chauhan
drankush@care.edu.in

1 School of Biological and Environmental Sciences, Shoolini University of Biotechnology and Management Sciences, Bajhol-Solan 173212, H.P., India

2 Faculty of Allied Health Sciences, Chettinad Academy of Research and Education, Chettinad Hospital and Research Institute, Kelambakkam, Chennai, Tamil Nadu 603103, India

3 King Abdullah Institute For Nanotechnology, King Saud University, P.O. Box 2455, Riyadh, Saudi Arabia

4 Department of Pharmacology, Chettinad Hospital and Research Institute, Chettinad Academy of Research and Education, Kelambakkam, Chennai, Tamil Nadu 603103, India

5 Department of Chemistry, Smt. Devkiba Mohansinhji Chauhan College of Commerce and Science, University of Mumbai, Dadra and Nagar Haveli (UT), Silvassa 396230, India

6 Department of Biomedical Sciences, Inha University College of Medicine, 100 Inha-ro, Michuhol-gu, Incheon 22212, Korea

7 Department of Physics, Sardar Patel University, Mandi 175001, H.P., India

Introduction

Nanotechnology is an interdisciplinary field of modern research dealing with the design, synthesis, and manipulation of particle structures ranging from approximately 1 to 100 nm (Chenthamara et al. 2019). Nanoparticles (NPs) have a wide range of applications in biomedical sciences, cosmetics, food industry, environmental health, chemical industries, etc. (Iravani et al. 2014). A variety of physical and chemical methods have been reported for the synthesis of NPs, but these are not widely used by scientists due to their high cost and toxic nature (Kumar et al. 2019; Sharma et al. 2020). Nowadays, the most popular method for the synthesis of NPs is the green synthesis method which involves plant extracts to produce NPs. Additionally, this method is a simple, safe, non-toxic, less costly, and environment-friendly method (Iravani et al. 2014; Marslin et al. 2018). Different types of metallic NPs have been prepared by the green synthesis method like magnesium oxide (MgO), silicon dioxide (SiO_2), titanium dioxide (TiO_2), zinc oxide (ZnO), copper oxide (CuO), silver oxide (AgO), and cuprous oxide (Cu_2O) from the leaf extract of *Manihot esculenta*, *Mentha arvensis, Cannabis sativa*, *Catha edulis,* flower extract of *Zephyranthes rosea*, fruit extracts of *Prunus serotine* and *Myrica esculenta,* respectively (Gebremedhn et al. 2019; Adinarayana et al. 2020; Ahmad et al. 2020; Chauhan et al. 2020; Essien et al. 2020; Maheshwaran et al. 2020; Kumar et al. 2021; Lal and Verma 2022). Among these NPs, the copper NPs are non-toxic and used in different fields like agricultural production, medicine, industrial engineering, photocatalysis, and the environment (Kasana et al. 2016; El-Saadony et al. 2020; Muthukumaran et al. 2020).

The Cu_2O-NPs of varying size, shape, and properties are synthesized by various methods like aqueous precipitation, organometallic decomposition, bio-reduction method, electrodeposition, and hydrothermal method (Ng and Fan 2006; Hayashi et al. 2018; Sharma et al. 2018; Muthukumaran et al. 2020). Moreover, Cu_2O-NPs have demonstrated excellent antimicrobial activity against *E. coli*, *S. aureus*, and *P. aeruginosa*. For example, Cu_2O-NPs synthesized from *Callistemon viminalis*, *P. serotine,* and *Musa acuminate* extracts have been reported in the literature for their excellent antibacterial activity (Li et al. 2016; Sharma et al. 2018; Muthukumaran et al. 2020; Kumar et al. 2021).

The *R. ellipticus,* commonly known as the Golden Himalayan raspberry, is an evergreen thorny shrub, native to China, Indonesia, the Indian subcontinent, and Sri Lanka (Lalla et al. 2018). Traditionally, the plant is used to treat fever, colic, cough, and sore throat (Muniyandi et al. 2019). The fruits of *R. ellipticus* are rich in various phenolic compounds, flavonoids, tannins, and steroids (Pandey and Bhatt 2016) and therefore reported for exhibiting antioxidant, antimicrobial, anti-proliferative, and anticancer activities (Saini et al. 2014; Muniyandi et al. 2019). Furthermore, Nasrollahzadeh et al. (2015) reported that phytochemical constituents of plants such as phenols and flavonoids play an important role in reducing the ions to nano-size and play an important role in the capping of NPs. Although *R. ellipticus* fruits are associated with a variety of phytochemicals and health benefits, no literature is available on the preparation of nanoparticles from its fruits. Therefore, the present work explored the application of *R. ellipticus* fruit extract as a capping and reducing agent for the synthesis of Cu_2O-NPs and evaluated in vitro antioxidant, antimicrobial, anticancer, and toxicity studies of *R. ellipticus* fruit-mediated Cu_2O-NPs.

Materials and methods

Sample collection and extract preparation

The fruits of *R. ellipticus* were collected from district Shimla (2000 m asl), Himachal Pradesh, India, in May 2018. The authentication of the plants was done in the Botanical Survey of India (BSI), Dehradun, India, with accession number 117. The collected fruits were dried at room temperature (20 to 25 °C) for 5–6 days, crushed in a grinder, and stored in airtight glass container for further analysis at room temperature.

The aqueous fruit extract was prepared by following the methodology of Chauhan et al. (2020). Using a shaking water bath, 5 g of dried fruit powdered sample was dissolved in 50 mL of double distilled water (ddH_2O) for 8 h at 60 °C. The extract was filtered through a Whatman filter paper 41, and dried in a hot air oven at 37 °C for 72 h. Further, aqueous fruit extract was stored at room temperature for further use.

Synthesis of Cu_2O-NPs from aqueous extract of *R. ellipticus* fruits

The Ru-Cu_2O-NPs were synthesized using copper (II) acetate as precursor salt and plant extract as a capping agent by following the methodology of Muthukumaran et al. (2020) with slight modification. The 5 g of copper (II) acetate was dissolved in 50 mL of water in a conical flask and then 30 mL of crude aqueous fruit extract was added to it with vigorous stirring for 30 min. The 10 mL of 0.05 M sodium hydroxide solution was slowly added to the prepared solution with constant stirring and heating at 80 °C for 2 h. As a result, the solution turned light green to brown, indicating the formation of nanoparticles (Fig. 1). The brown
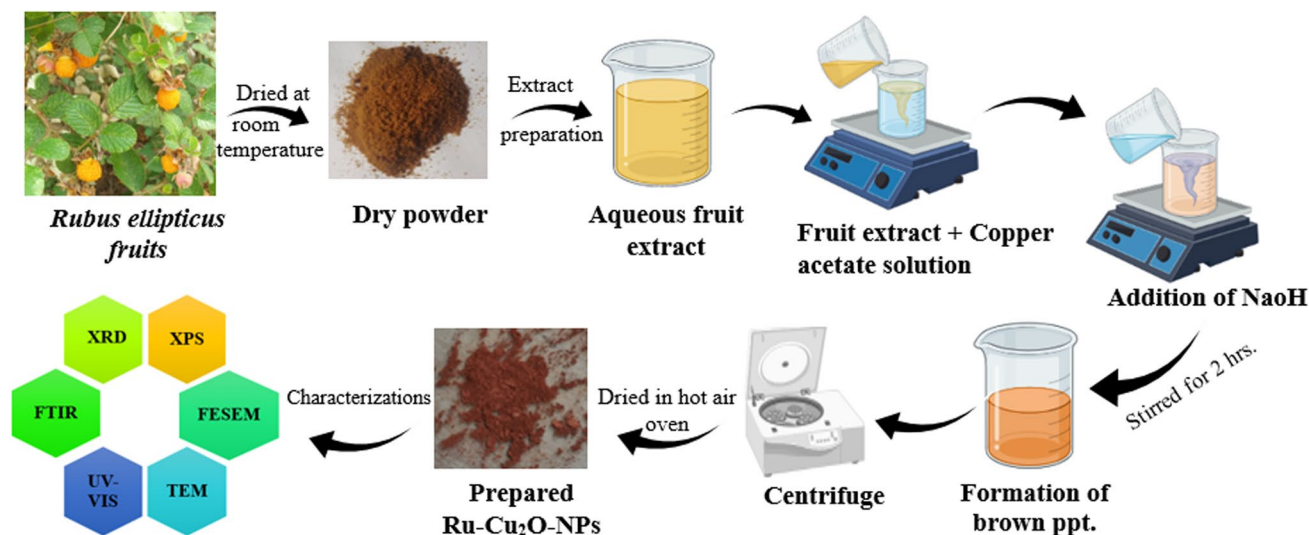
Fig. 1 Flow chart for the synthesis of Ru-Cu$_2$O-NPs

precipitates were collected, centrifuged, and washed with deionized water for the removal of impurities. The sample was recollected after washing, dried at 50 °C for 24 h, and stored in Eppendorf tubes at room temperature for further use.

Characterizations of *R. ellipticus* fruits extract-mediated nanoparticles (Ru-Cu$_2$O-NPs)

The X-ray diffraction spectroscopy (XRD) was performed using Ringaku Minifiex 600, Japan X-ray powder diffractometer with CuKα radiation (λ = 1.5405Å) operating at 30 kV, at room temperature. The diffraction measurement was taken between 15° and 65° at a scanning rate of 2°/min for the determination of the structural phase and crystalline nature of the material. The Fourier transform infrared spectroscopy (FTIR) for functional group identification was performed using a 400 FT-IR/FIR spectrometer (make: PerkinElmer, USA) within the range 400 cm^{-1}–4000 cm^{-1}. X-ray photoelectron spectroscopy (XPS) for the determination of elemental composition, chemical state, and electronic state of the elements in the material was performed using a Thermo Fisher Scientific X-ray photoelectron spectrometer (model: Nexa Base). Field emission scanning electron microscopy (FE-SEM) was performed using SU 8010 series (make: Hitachi, Japan) with an operating voltage of 5 kV for the determination of morphology. Transmission electron microscopy (TEM) was performed to determine the particle size and cross-sectional morphology using JEOL JEMA 2100 field emission transmission electron microscope (Japan). The UV–Vis spectroscopy was performed

using a Perkin Elmer UV–Vis spectrophotometer (model: UV-2450).

In vitro antioxidant activity of Ru-Cu$_2$O-NPs

DPPH (2,2-diphenyl-1-picryl-hydrazyl-hydrate) assay

The DPPH free radical scavenging activity of the aqueous fruit extract and Ru-Cu$_2$O-NPs was measured by following Mensor et al. (2001) methodology with few modifications. The 0.1 mL of aqueous fruit extract/Ru-Cu$_2$O-NPs in different concentration (20–100 µg/1 mL) was separately mixed with 0.9 mL of DPPH (0.004% in methanol, w/v) in test tubes. The mixtures were allowed to react at room temperature. After 30 min of incubation, the discolouration of the purple colour was recorded at 510 nm using an UV–Vis spectrophotometer in triplicate. Methanol served as blank and ascorbic acid was used as a positive control. The radical scavenging activity was calculated as follows:

$$DPPH\ activity\ (\%) = \frac{\left[Control\ (Abs) - Test\ sample\ (Abs)\right]}{Control\ (Abs)} \times 100$$

ABTS (2,2'-azino-bis (3-ethylbenzothiazoline-6-sulfonic acid)) assay

The antioxidant effect of the aqueous fruit extract and Ru-Cu$_2$O-NPs was observed using the ABTS radical cation decolourization assay of Shirwaikar et al. (2006). First, 7 mM of ABTS solution was mixed with 2.45 mM ammonium persulphate in equal quantities and allowed to react

for 16 h at room temperature in the dark. After that 0.1 mL of aqueous fruit extract/Ru-Cu$_2$O-NPs in each concentration (20–100 μg/mL) were mixed with 0.9 mL of ABTS solution in test tubes. The reaction mixtures were incubated in the dark condition for 30 min. Here, methanol and ascorbic acid were used as a blank and as a positive control, respectively. The absorbance was taken at 745 nm using an UV–Vis spectrophotometer in triplicate and percent inhibition was calculated by using the formula:

$$ABTS\ assay(\%) = \frac{\left[Control\ (Abs) - Test\ sample\ (Abs)\right]}{Control\ (Abs)} \times 100$$

FRAP free radical scavenging assay

The free radical scavenging activity of Ru-Cu$_2$O-NPs and aqueous fruit extract at different concentrations (20–100 μg/mL) was analysed through a ferric ion reducing antioxidant power (FRAP) assay by following the methodology of Banerjee et al. (2008). In this procedure, 1 mL of Ru-Cu$_2$O-NPs in different concentration (20–100 μg/mL) was mixed separately into the test tube with 1 mL of sodium phosphate buffer (0.2 M in dH$_2$O; pH 6.6). After that 1 mL of 1% potassium ferricyanide was added to the test tubes and incubated for 20 min in a water bath at 50 °C. Afterwards, 1 mL of the reaction mixture from each sample was taken and 1 mL of dH$_2$O was added. Each test tube was then filled with 0.2 mL of ferric chloride (0.1% in distilled water) solution. At the end of the process, 200 μL of solution were poured into 96-wells microtitre plate from each test tube. The results were recorded in triplicate and repeated for the aqueous fruit extract. The blank was prepared similarly, except dH$_2$O was replaced by the 1% potassium ferricyanide. The ascorbic acid (20–100 μg/mL) was used as a positive control. The antioxidant capacity of each sample was calculated using the ferrous sulphate linear calibration curve and expressed as FeSO$_4$ equivalents.

IC$_{50}$ value determination

A linear regression analysis of plots of different concentrations of the test sample against the mean percentage of antioxidant activity calculated from triplicate assays was used to determine the IC$_{50}$ value for all antioxidant assays.

In vitro antimicrobial activity

Selection of strains

For the antibacterial assay, two strains of Gram-positive bacteria [*Staphylococcus aureus* (MTCC 731), *Bacillus subtilis* (MTCC 441)], and two strains of Gram-negative bacteria [*Pseudomonas aeruginosa* (MTCC 424), *Escherichia coli* (MTCC 739)] were selected, whereas for antifungal assay two pathogenic strains of fungi [*Fusarium oxysporum* (SR266-9) and *Rosellinia necatrix*; (HG964402.1.)] were selected. The bacterial and fungal strains were obtained from CSIR-Institute of Microbial Technology (IMTech), Chandigarh, and the School of Microbiology, Shoolini University, Solan, respectively.

Disc diffusion assay for determination of antibacterial activity

The antibacterial activity of crude aqueous fruit extract of *R. ellipticus* and Ru-Cu$_2$O-NPs was observed by using the disc diffusion method of Bauer (1966). The 100 μL of each bacterial culture (OD ~ 0.1) with the help of sterile cotton swabs was uniformly spread on the surface of the nutrient agar (NA) plates. In the next step, from stock solutions (10 mg/mL in 10 % DMSO), aqueous fruit extract (300 μg/mL per disc) was separately poured on 6 mm discs in the NA plate. The plate was then placed in the refrigerator for 2 h. In the last step, the plate was incubated at 37 °C for 24 h in an incubator. As a positive and negative control, ampicillin (0.100 mg/mL) and DMSO (10%) were used against all tested strains, respectively. The zone of inhibition was measured in mm with an antibiotic zone scale. The results were obtained in triplicate and method was repeated separately with Ru-Cu$_2$O-NPs (300 μg/mL per disc).

Poison food technique (PFT) for determination of antifungal activity

The PFT was used to determine the antifungal activity of aqueous fruit extract and Ru-Cu$_2$O-NPs by following the protocol of Grover and Moore (1962). First, each fungal strain was placed on Petri plates containing potato dextrose agar (PDA) media and aqueous fruit extract (300 μg/mL per plate) and incubated at 25 °C for 7 days. After incubation, the colony diameter was measured through an antibiotic zone scale. Media without the extract was used as a negative control and hygromycin-B (0.100 mg/mL in dH$_2$O) was used as a positive control. The antifungal activity of aqueous fruit extract was expressed in terms of percentage inhibition and calculated by using the following formula:

$$Inhibition\ (\%) = \frac{C - T}{C} \times 100$$

where, C is the diametric growth of the colony in control, T is the diametric growth in the aqueous fruit extract.

This method was repeated separately with Ru-Cu$_2$O-NPs (300 µg/mL per plate) and data were recorded.

Minimum inhibitory concentration (MIC)

The microtitre broth dilution method given by the Clinical and Laboratory Standards Institute (Clinical and Laboratory Standards Institute 2012) was used for evaluating MIC values for antibacterial and antifungal assays. The 100 µL of the aqueous fruit extract/Ru-Cu$_2$O-NPs (20 mg/mL in 10% DMSO) was mixed with NB/PDB in a 96-wells microtitre plate. Serial dilution of extracts was made in such a way that the next well had half the concentration from the previous well. The 10 µL of each bacterial/fungal strain solution (OD ~ 0.1) was added separately to the well of the microtitre plate and then incubated for 24 h at 37 °C (for bacteria) and 48 h at 25 ± 2 °C (for fungi) in an incubator. After incubation, 15 µL of resazurin (0.04% in dH$_2$O) solution was added to wells as an indicator. A colour change in the well was observed visually.

In vitro toxicity analysis of Ru-Cu$_2$O-NPs

Cytotoxicity on stem cell lines and cancer cells

Cell source and culture A 4,5-dimethylthiazol-2-yl-2,5-diphenyl tetrazolium bromide (MTT) assay was used to evaluate the in vitro toxicity of nanoparticles (Kang et al. 2013). Bone marrow-derived mesenchymal stem cells (BM MSCs) were purchased from CEFOBIO (80 M-20–023) and human chondrocytes (HC) were from Ajou University, South Korea (IRB approval number: AJIRB-GN3-07–102). The BM MSCs were cultured on CEFOgro Human MSC Growth Medium (CEBO bio), whereas HC cells were cultured on high glucose Dulbecco's modified Eagle' (HG DMEM; Hyclone) with 10% foetal bovine serum (FBS; Gibco) at 37 °C.

MTT cell-proliferation assay The MTT assay was done by following the methodology of Kang et al. (2013). The BM MSCs and HM cells were cultured in 96-wells plate at a density of 1×10^4 cells/mL and incubated at 37 °C for 24 h under 5% CO$_2$. The next day, the cells were treated with Ru-Cu$_2$O-NPs at different concentrations (1.5–100 µg/ml) for 24 h and 48 h, followed by an MTT assay (4 h incubation at 37 °C) to assess the cell viability. Using a microplate reader, the optical density was noted at 570 nm in triplicate.

Cytotoxicity on cancer cell lines

Cell source and culture Adherent colon cancer cell lines (SW480 and SW620) were purchased from the National Centre for Cell Science (NCCS), Pune, India. These are the paired colon cancer cell lines isolated from the primary site and metastatic lymph node of the same patient, respectively. The cell cultures were expanded in standard DMEM (low glucose, Glutamax supplement) (Cat. No. 10567014, GIBCO, USA) supplemented with 10% FBS (Cat. No. 10270106, GIBCO, Brazil), 1% Antibiotic–Antimycotic (Cat. No. 15240062, GIBCO, USA) at 37ºC under normoxic condition.

CCK8 analysis 5000 cells/well of primary and metastatic colon cancer cells (SW480 and SW620 cells, respectively) were seeded in a 96-wells plate. The cells were treated with various concentrations (1.5–100 µg/mL) of Ru-Cu$_2$O-NPs. After 48 h of treatment, 10 µL of CCK8 reagent (Cat. No. 96992, Sigma–Aldrich) was added to the cells and incubated for 4 h. The absorbance was measured at 450 nm, and the percentage of cell viability was calculated, and graphs were plotted.

EZBlue cell assay kit The 5000 cells/well of primary and metastatic colon cancer cells (SW480 and SW620 cells, respectively) were seeded in a 96-wells plate. The cells were treated with various concentrations of nanoparticles ranging from 1.5 to 100 µg/mL. After 48 h of treatment, 10 µL of EZBlue solution (Cat. No. CCK004–2500, Himedia) was added to the cells and incubated for 6–8 h. The absorbance was measured at 580 and 630 nm, and the percentage of cell viability was calculated, and graphs were plotted.

Morphological analysis 2×10^4 cells/well of primary colon cancer cells (SW480) and metastatic colon cancer cells (SW620) were seeded in a 6-well plate and allowed for culture expansion. After 24 h of culture, the spent medium was removed and cells were treated with a 12.5 µg/mL concentration of nanoparticle supplemented DMEM medium. After 48 h of the treatment, the images of the cell morphology after treatment were captured and the changes in cell morphology were analysed.

Statistical analysis

All the data were statistically analysed using SPSS software through the paired sample t-test analysis. The results were expressed in mean ± standard error mean.

Results and discussion

Structural and crystallographic study of Ru-Cu$_2$O-NPs

The XRD pattern of Ru-Cu$_2$O-NPs is given in Fig. 2 (a), which exhibits the six prominent diffraction peaks at

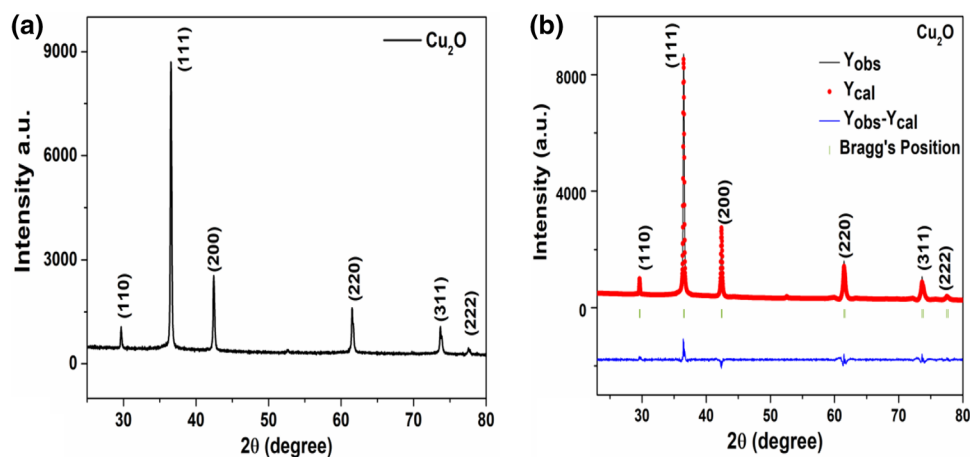**Fig. 2** (**a**) XRD pattern and (**b**) Rietveld refined XRD patterns of Ru-Cu$_2$O-NPs

Table 1 Structural and Rietveld refine parameters of Ru-Cu$_2$O-NPs

Sample	Ru-Cu$_2$O-NPs
Structure	Cubic cuprite
Space group	Pn-3 m
a (Å)	4.263280
b (Å)	4.263280
c (Å)	4.263280
Volume (Å)^3	77.487
χ^2	2.62
R_p	18.8
R_{wp}	16.2
R_e	10
Average crystallite size (Scherrer method) (nm)	25

29.61, 36.47, 42.36, 61.46, 73.63, and 77.45 corresponding to (110), (111), (200), (211), (311), and (222) *hkl* planes, respectively (Kerour et al. 2018). The intense diffraction peaks in the XRD patterns of the RF-Cu$_2$O-NPs confirmed the high crystallinity of the prepared samples without any secondary phases and are in good agreement with the JCPDS no. 05–0667. The particle size of the synthesized nanoparticles is given in Table 1 and was calculated using the Scherrer formula given in Eq. (1) (Chauhan et al., 2020):-

$$D = \frac{0.9\lambda}{\beta \mathrm{Cos}\theta} \tag{1}$$

where, D is the average crystallite size, λ is the X-ray wavelength, θ is the Bragg angle, and β is the full width at half maximum FWHM. The XRD pattern was refined using the Fullprof programme using the spacegroup Pn-3 m. Pseudo-Voigt profiles were used to define peak patterns, and linear interpolation was used to fit the backdrop. Global parameters including backdrop, instrumental, and scale factors were

refined first, followed by cell parameters. Finally, sequentially refined the FWHM parameters, shape parameters, preferred orientation, and atomic positions were refined sequentially. The Rietveld refinement confirms the cubic cuprite structure of the synthesized Cu$_2$O-NPs, and calculated parameters are provided in Table 1.

XPS study

The XPS analysis was carried out to determine the oxidation states of the surface species of the Ru-Cu$_2$O-NPs. The Cu 2p XPS spectra show the two most prominent peaks at binding energies 952.30 eV, and 932.45 eV, respectively, corresponding to Cu2p$_{1/2}$ and Cu2p$_{3/2}$ (Wang et al. 2015). The deconvolution of these two peaks reveals the presence of Cu^{2+} ions, whose peaks appear at 953.02 eV and 933.62 eV, and a higher concentration of Cu^{1+} ions (Fig. 3). The presence of the electronic shakeup satellite peaks in the XPS spectra of Cu2p confirms the presence of the CuO or Cu^{2+} on the surface of the Cu$_2$O octahedra, which confirms the presence of CuO and Cu$_2$O on the surface of the octahedral (Jiang et al. 2013; Azimi et al. 2014). The amount of Cu^{2+} on the surface of the octahedra is higher due to its exposure to oxygen. The asymmetric oxygen 1 s spectra can be resolved into four different components revealed by the Gaussian fitting, i.e., O$_L$, which consists of lattice oxygen attached to CuO and Cu$_2$O present on the surface of Cu$_2$O octahedra with binding energies 529.92 eV and 530.4 eV. The O$_V$ with binding energy 531.54 eV is attributed to the oxygen vacancies in the lattice of surface CuO and Cu$_2$O species. The component at a higher binding energy of 532.26 eV is attributed to the surface chemisorbed, disassociated oxygen species, and hydroxyl species (Wang et al. 2015). The higher percentage of O$_C$ on the surface of the Cu$_2$O octahedra reveals the strong ability of the octahedra to adsorb oxygen. This

Fig. 3 Cu2p and O1s core shell level XPS spectra of Ru-Cu$_2$O-NPs
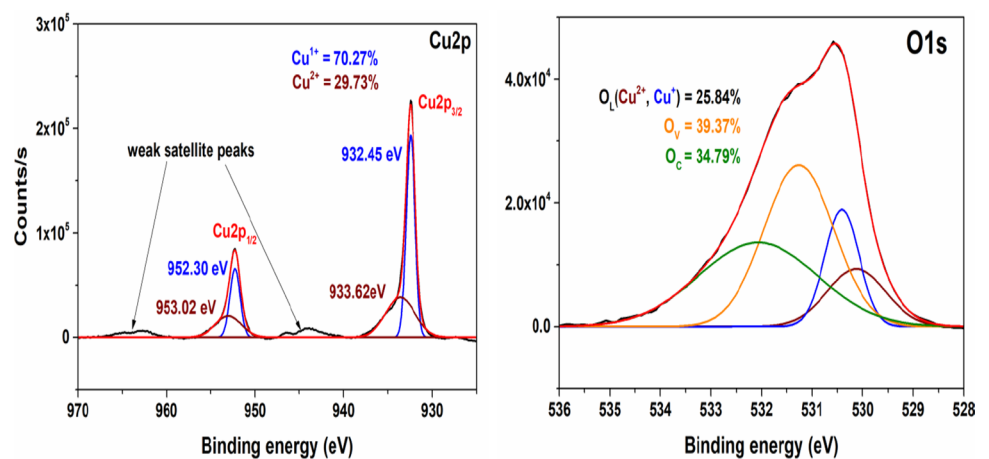
component plays an important role in the NPs antimicrobial and photocatalytic degradation capability (Chauhan et al. 2021).

FE-SEM analysis with mapping

Figure 4 shows the FE-SEM micrographs of Cu$_2$O octahedral at 500 nm magnification. The morphology depicts the formation of octahedral from the self-assembled Cu$_2$O-NPs. The elemental mapping reveals a higher concentration of copper species than oxygen. This may be possible due to the existence of Cu$_2$O and CuO species on the surface of the Cu$_2$O octahedral, as confirmed by the XPS analysis.

Morphology characterization of Ru-Cu$_2$O-NPs by TEM

It can be observed in Fig. 5a, b that the smaller particles with an average particle size of 9.72 ± 0.6 nm self-assembled to form the larger grains with an average grain size of
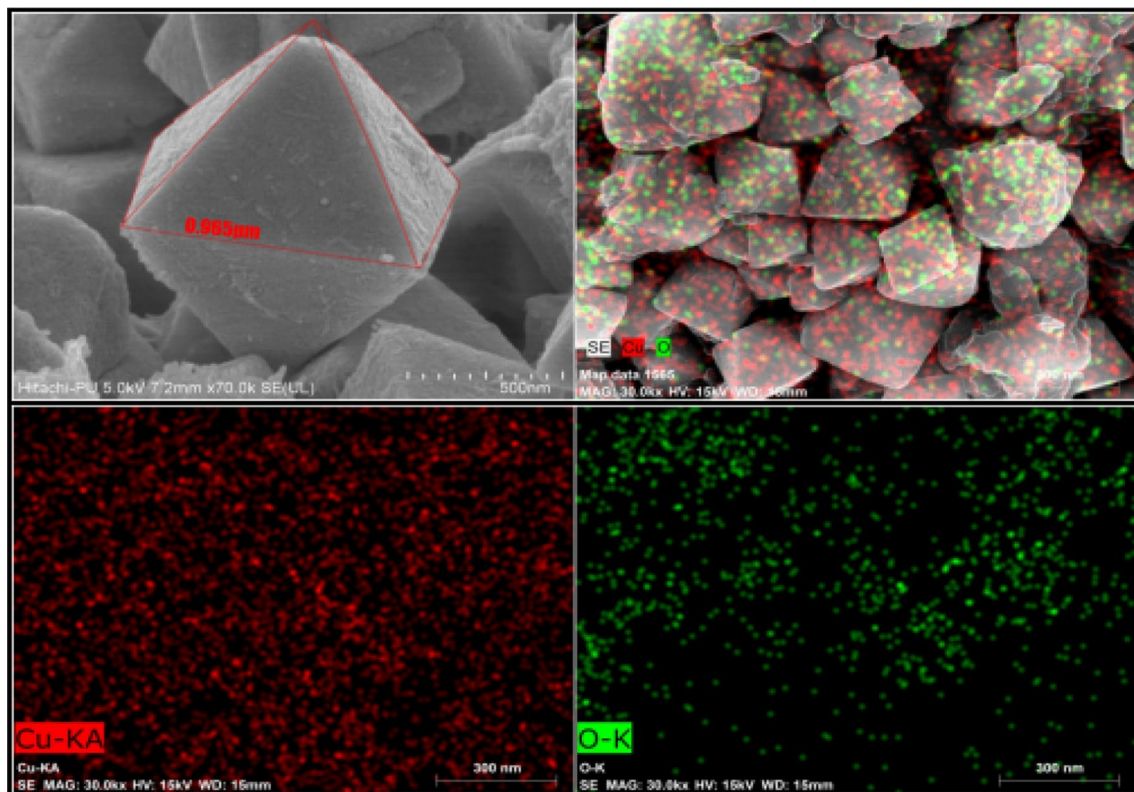
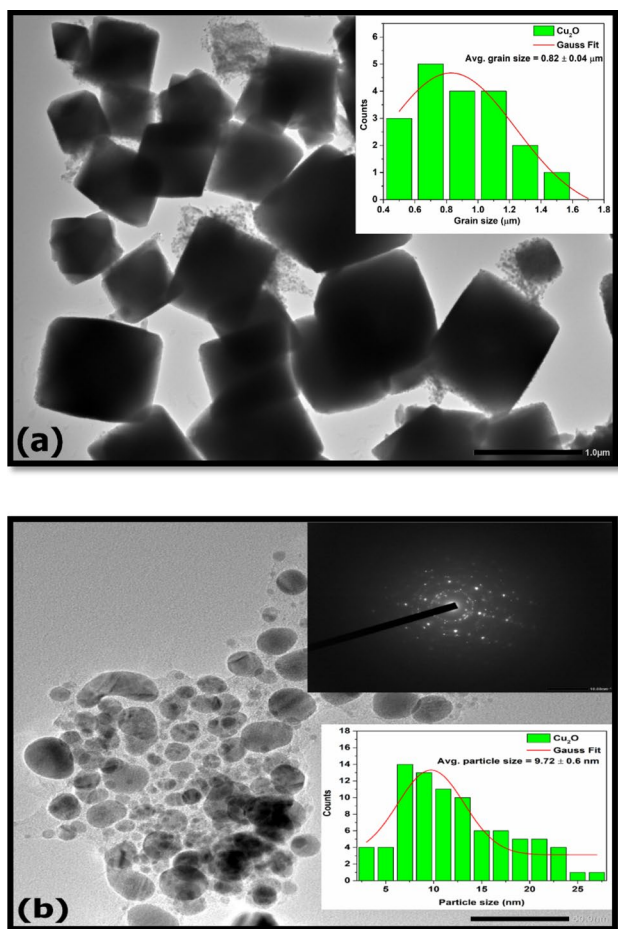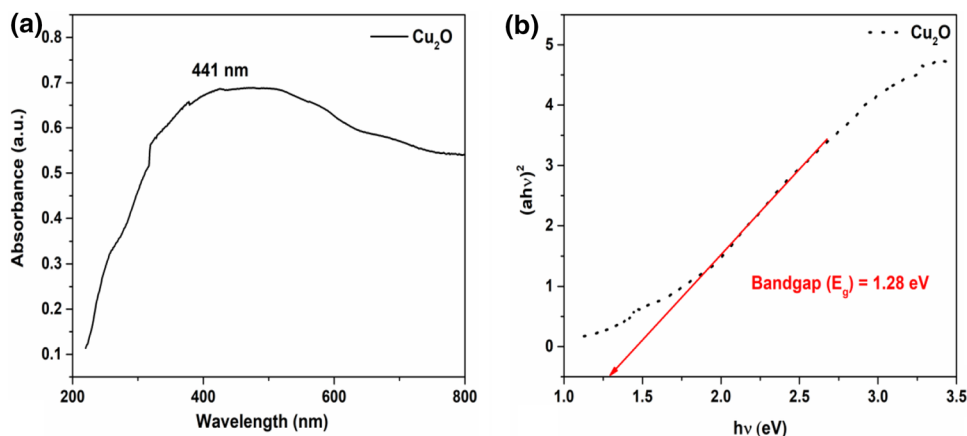**Fig. 4** FE-SEM micrographs and elemental mapping of Ru-Cu$_2$O-NPs

Fig. 5 (**a**) TEM micrograph at 1 μm scale with grain size distribution (**b**) TEM micrograph at 50 nm scale, particle size distribution, and SAED pattern of Ru-Cu_2O-NPs

0.82 ± 0.04 μm. In the SAED pattern shown in Fig. 5b the presence of bright fringes reveals the existence of the single crystalline Cu_2O octahedral, and the presence of diffused rings also reveals the existence of NPs in the polycrystalline

phase. This mixed SAED pattern is due to polycrystalline Cu_2O-NPs and single-crystalline Cu_2O octahedral.

UV–Vis analysis

UV spectroscopy analysis was employed to determine the synthesized NPs absorbance peak and optical bandgap. It can be seen in Fig. 6a that the maximum absorption peak of Cu_2O octahedra is present at 441 nm, which follows the given literature (Thoka et al. 2019). The direct optical bandgap (Eg) given in Fig. 6b was determined using the Tauc's relation (Pankove 1975; Chauhan et al. 2021):-

$$(\alpha h\nu)^2 = A(h\nu - Eg) \tag{2}$$

where, α is the absorption coefficient, and $h\nu$ is corresponds to the photon energy. Hence, the plot between $(\alpha h\nu)^2$ and $(h\nu)$ gives the energy bandgap (E_g).

FTIR-study

The FTIR spectra of Ru-Cu_2O-NPs shown in Fig. 7 exhibit three strong absorption bands at 635 cm^{-1}, 1089 cm^{-1}, and 3420 cm^{-1} which corresponds to Cu–O bond stretching, vibrational modes of nitrate ions, and O–H stretching vibrations due to the presence of alcoholic and phenolic hydroxyl groups (Shelari and Katkar 2018; Zhou et al. 2019). The peak observed at 1633 cm^{-1} is the –OH bending vibrations that emerge from the surface adsorbed water molecules (Zhang et al. 2014). The band at 2932 cm^{-1} is attributed to the symmetric and asymmetric CH_2 stretching, respectively (Li et al. 2016).

Antioxidant activity

The antioxidant potential of aqueous fruit extract, Ru-Cu_2O-NPs, and ascorbic acid (control) analysed through DPPH, ABTS, and FRAP assays, and the results are presented in

Fig. 6 (**a**) Absorbance spectra and (**b**) optical bandgap of Ru-Cu_2O-NPs

Table 2 Antioxidant activity of aqueous fruit extract and Ru-Cu$_2$O-NPs

| Antioxidant assays	Concentration (μg/mL)	Ru-Cu$_2$O-NPs	Aqueous fruit extract	Ascorbic acid
DPPH (% Inhibition)	20	42.29 ± 0.8	45.3 ± 1.2	50.9 ± 0.8
	40	48.2 ± 0.4	53.7 ± 0.9	58.3 ± 0.4
	60	54.3 ± 0.8	60.3 ± 0.9	64.4 ± 0.5
	80	59.4 ± 0.5	72.8 ± 0.5	73.4 ± 0.4
	100	64.8 ± 0.8	79.2 ± 0.8	79.3 ± 0.5
ABTS (% Inhibition)	20	38.5 ± 0.4	41.1 ± 0.6	46.6 ± 0.5
	40	45.9 ± 0.4	51.1 ± 0.7	55.3 ± 0.2
	60	53.2 ± 0.3	58.6 ± 0.6	63.7 ± 0.4
	80	57.9 ± 0.9	67.0 ± 0.5	74.4 ± 0.5
	100	61.3 ± 0.5	74.9 ± 0.6	79.4 ± 0.5
FRAP (μM/mL FeSO$_4$ equivalents)	20	16.6 ± 0.6	25.9 ± 0.3	40.9 ± 0.6
	40	28.1 ± 0.2	31.0 ± 0.5	48.9 ± 1.6
	60	37.4 ± 0.5	38.7 ± 0.7	55.5 ± 1.2
	80	43.4 ± 0.2	49.8 ± 0.5	59.3 ± 1.3
	100 μg	51.2 ± 0.5	57.4 ± 0.4	64.5 ± 1.5
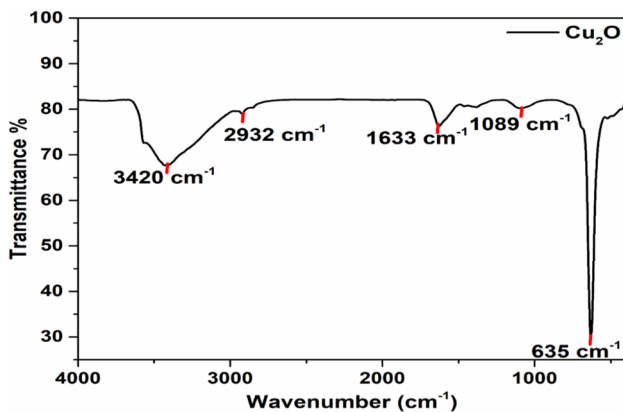
Fig. 7 FTIR spectra of Ru-Cu$_2$O-NPs

Table 2 and Fig. 8. The results showed the increase in free radical's percentage inhibition with an increased concentration (20–100 μg/mL) of aqueous fruit extract and Ru-Cu$_2$O-NPs from 20–100 μg/mL (Table 2). For all antioxidant assay, the aqueous fruit extract (DPPH-79.2%, ABTS-74.9%, and FRAP-57.4 μM/mL FeSO$_4$ equivalents) showed higher percentage inhibition than Ru-Cu$_2$O-NPs (DPPH-64.8%, ABTS-61.3%, and FRAP-51.2 μM/mL FeSO$_4$ equivalents) at concentration of 100 μg/mL (Table 2). Similarly, the highest antioxidant potential ($p < 0.05$) in terms of lowest IC$_{50}$ value was observed in aqueous fruit extract (DPPH: 31.6 ± 1.3 μg/mL, ABTS: 39.2 ± 1.1 μg/mL, and FRAP: 82.8 ± 0.6 μM Fe^{2+} equivalent) than Ru-Cu$_2$O-NPs (DPPH: 46.2 ± 1.5 μg/mL, ABTS: 55.2 ± 0.3 μg/mL, and FRAP: 94.5 ± 0.4 μM Fe^{2+} equivalent) (Fig. 8). Therefore, present study revealed

Fig. 8 In vitro antioxidant activity (IC$_{50}$ value) of Ru-Cu$_2$O-NPs and aqueous fruit extract [Different superscript showed significant ($p < 0.05$) difference between (**a**) aqueous fruit extract, (**b**) Ru-Cu$_2$O-NPs, and (**c**) ascorbic acid]
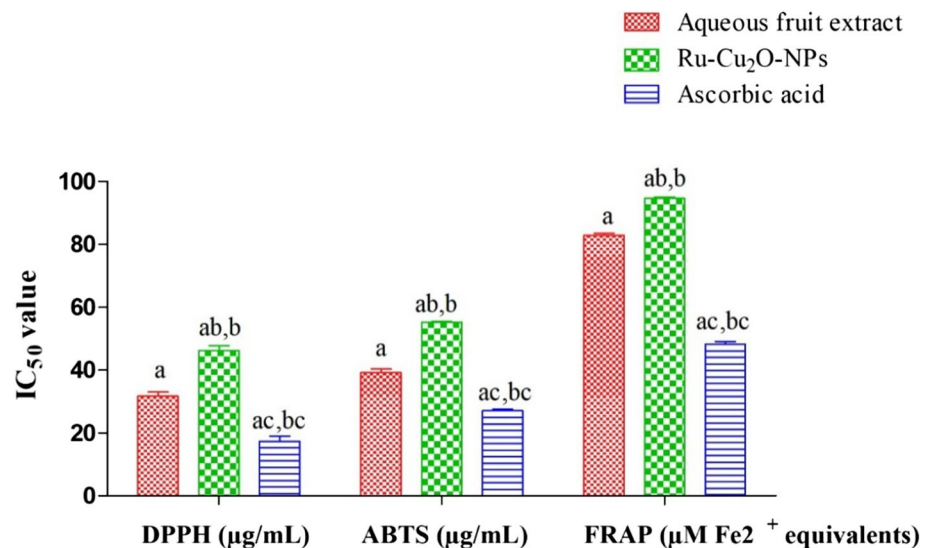
that in all assays, ascorbic acid followed by aqueous fruit extract showed the lowest IC_{50} value compared to $Ru-Cu_2O$-NPs. Lower IC_{50} values indicate higher antioxidant activity in the literature (Fidrianny et al. 2015). It means fruits has a higher antioxidant potential than nanoparticles. This could be due to the presence of higher ascorbic acid content and polyphenolic compounds in the aqueous fruit extract of *R. ellipticus*.

Mahendran and Kumari (2016) and Reddy et al. (2014) also observed higher antioxidant activity of fruit extracts of *Nothapodytes nimmoniana* and *Piper longum* compared to green-synthesized NPs. According to the authors, the higher antioxidant potential of the crude extracts might be attributed to a larger concentration of phenolic components in the crude extract (Moller et al. 1999; Sannigrahi et al. 2010). The CuO-NPs synthesized from the plant extract of *Tinospora cardifolia*, *Abutilon indicum*, *Allium sativum, Azadirachta indica*, and *Moringa oleifera* also exhibited potent in vitro antioxidant activity with IC_{50} values of 566 µg/mL, 84 µg/mL, 40.52 µg/mL, 34 µg/mL, and 34.82 µg/mL, respectively (Nethravathi et al. 2015; Rehana et al. 2017; Ijaz et al. 2017; Velsankar et al. 2020).

Antimicrobial activity

To evaluate antibacterial activity, the $Ru-Cu_2O$-NPs and aqueous fruit extract of *R. ellipticus* were tested against two Gram-positive (*S. aureus* and *B. subtilis*) and two Gram-negative (*E. coli* and *P. aeruginosa*) bacteria. The disk diffusion assay and MIC results are presented in Figs. 9, 10. The results clearly showed maximum growth inhibition of all bacteria through $Ru-Cu_2O$-NPs. The maximum antibacterial activity (ZOI in mm and MIC in µg/mL) of $Ru-Cu_2O$-NPs was observed against *B. subtilis* (20 ± 0.5 mm and 7.81 µg/mL) followed by *S. aureus* (16 ± 1 mm and 15.62 µg/mL), *P. aeruginosa* (15 ± 0.5 mm and 31.25 µg/mL), and *E. coli* (14 ± 0.5 mm and 31.25 µg/mL) (Fig. 9 and Table 3). Whereas aqueous fruits extract showed higher activity against *E. coli* (10 ± 1 mm; 250 µg/mL), followed by *P. aeruginosa* (9.5 ± 0.5 mm; 250 µg/mL) and *S. aureus* (9 ± 0.5 mm; 500 µg/mL, and *B. subtilis* (8.5 ± 0.5 mm; 500 µg/mL) (Figs. 9, 10). Compared to aqueous fruit extract, the synthesized NPs have shown good antibacterial activity against both Gram-positive and Gram-negative bacteria, which were almost similar to the positive control (ampicillin) (Fig. 9). A significant variation ($p < 0.05$) was observed

Fig. 9 Antibacterial activity of aqueous fruit extract and Ru-Cu_2O-NPs against pathogenic bacteria [Different superscripts showed significant ($p < 0.05$) difference between (**a**) aqueous fruit extract, (**b**) Ru-Cu_2O-NPs and (**c**) ascorbic acid]
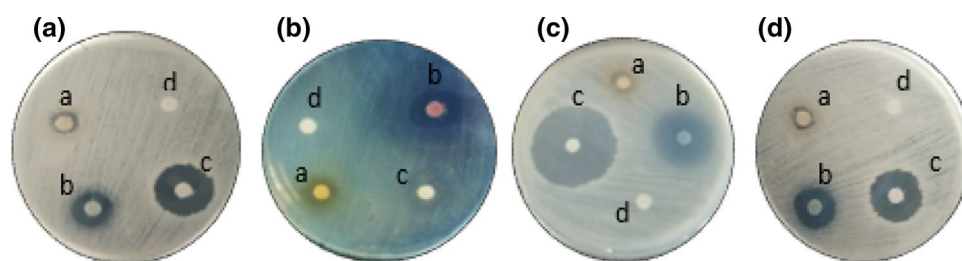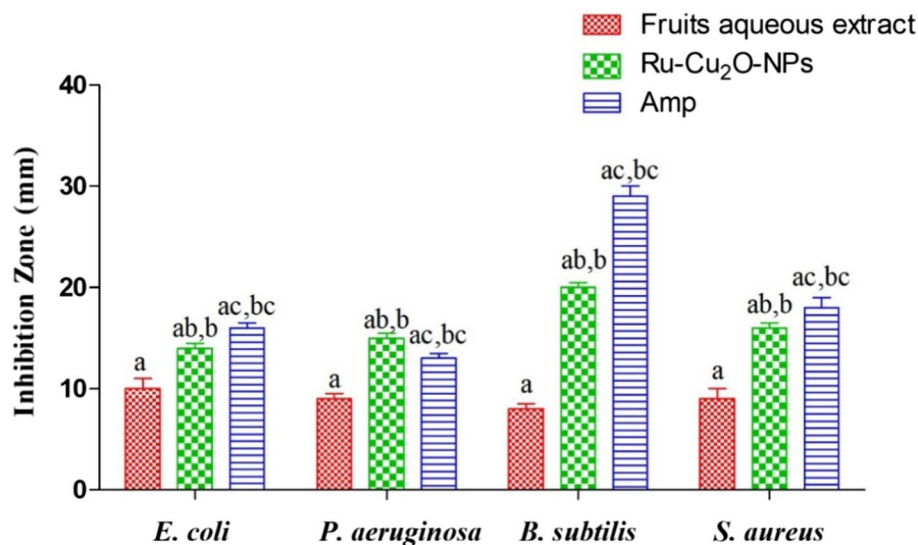

Fig. 10 Petri plates showing zone of inhibition [(a-300 µg/mL, aqueous fruit extract; b-300 µg/mL, Ru-Cu_2O-NPs; c-50 µg, Ampicillin; d-negative control (DMSO-10 µL)] of aqueous fruit extract and Ru-Cu_2O-NPs against *E. coli* (**A**), *P. aeruginosa* (**B**), *B. subtilis* (**C**), *S. aureus* (**D**)

Table 3 MIC of Ru-Cu$_2$O-NPs and plant extract

Microbial strains	MIC (μg/mL)		
	Aqueous fruit extract	Ru-Cu$_2$O-NPs	Positive control
E. coli	250	31.25	6.25
P. aeruginosa	250	31.25	6.25
B. subtilis	500	7.81	1.56
S. aureus	500	15.62	3.12
F. oxysporum	125	31.25	–
R. necatrix	62.5	7.81	–

between the Ru-Cu$_2$O-NPs and aqueous fruits extract through the paired sample t-test analysis. The present study results were similar to the results of Hussien et al. (2019), Regmi et al. (2019), and Bezza et al. (2020) where plant-mediated NPs showed higher antibacterial potential than plant extracts. The antibacterial activity of green synthesized nanoparticles could be due to the ability of plant extract to act as a capping and reducing agent that reduces particle size and enhances the antimicrobial efficacy of nanoparticles (Moharekar et al. 2014; Ramesh et al. 2021).

The antifungal activity of aqueous fruit extract and Ru-Cu$_2$O-NPs was determined by the food poison technique and MIC assay against *F. oxysporum* and *R. necatrix*. The results showed significantly ($p < 0.05$) stronger inhibition (%) of *R. necatrix* (80.6 % and 7.81μg/mL) than *F. oxysporum* (51.6 % and 31.25 μg/mL) with Ru-Cu$_2$O-NPs compared to the control. However, the aqueous extract of fruits showed lower percentage inhibition of both fungi (Figs. 11, 12). In the literature, the Ru-Cu$_2$O-NPs also showed potent antifungal activity (MIC) against *F. oxysporum* f. sp. *carthami* (0.06 mg/mL), *F. oxysporum* f. sp. *ciceri* (0.03 mg/mL), and *F. oxysporum* f. sp. *udum* (0.06 mg/mL) (Shende et al. 2016).
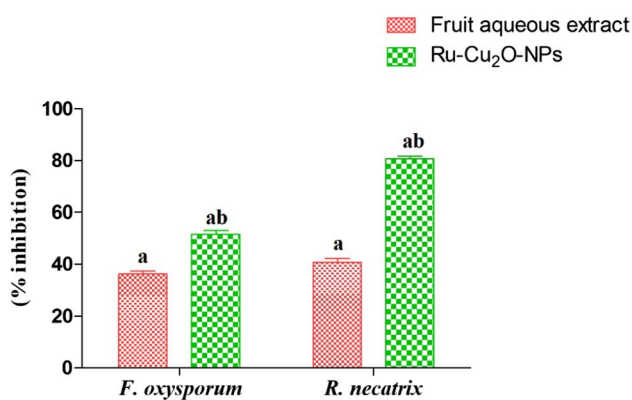

Fig. 11 Graphical representation of plant extract and Ru-Cu$_2$O-NPs against plant pathogenic fungus [Different superscripts showed significant ($p < 0.05$) difference between (a) aqueous fruit extract and (b) Ru-Cu$_2$O-NPs]
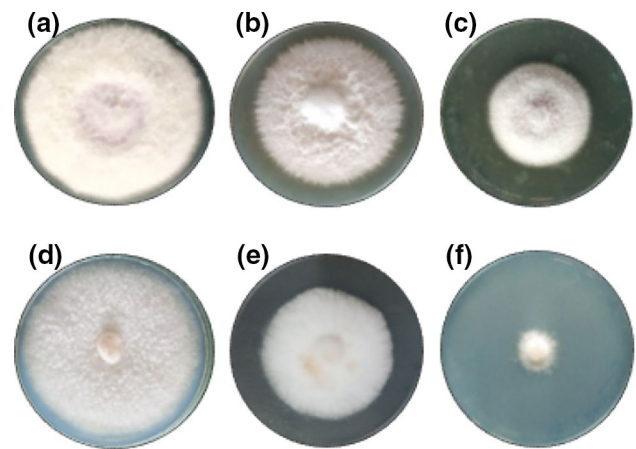

Fig. 12 Petri plates showing percentage inhibition of aqueous fruit extract and Ru-Cu$_2$O-NPs against *F. oxysporum* and *R. nectarix*; **a** and **d**- *F. oxysporum* and *R. nectarix* Control (Without extract and NPs), **b** and **e**-Aqueous fruit extract (300 μg/mL), **c**- and **f**- Ru-Cu$_2$O-NPs (300 μg/mL)

Similarly, Viet et al. (2016) also observed good antifungal activity of copper nanoparticles against *Fusarium* species (93.98%).

The probable mechanism of antimicrobial activity of Ru-Cu$_2$O-NPs is presented in Fig. 13. The antimicrobial activity of the Ru-Cu$_2$O-NPs could be due to the release of metal (Cu^{1+}/Cu^{2+}) ions in aerobic circumstances, which exhibit toxicity to the microbe. The nanoparticles serve as transporters and deliverers of metal ions for interaction with microorganisms, with metal (Cu^{1+}/Cu^{2+}) ions exerting the main antimicrobial effects. The Cu^{1+}/Cu^{2+} ions bind to the cell wall, which lead to the disruption cell membrane integrity and the production of reactive oxygen species (ROS), including hydrogen peroxide. Aside from these effects, hydrogen peroxides destabilize proteins and enzymes, dysfunction mitochondria, disassemble ribosomes, and impair cell viability overall (Zhao et al. 2015; Dhatwalia et al. 2022).

In vitro toxicity of Ru-Cu$_2$O-NPs

The in vitro toxicity analysis of Ru-Cu$_2$O-NPs was also done on two normal human cell lines (BM MSCs and HC) for 24' h and 48' h of treatments (Fig. 14). The result showed that after 24' h and 48'h of treatments on BM MSCs, a non-significant ($p > 0.05$) reduction in cell proliferation was observed up to 50 μg/mL concentration of Ru-Cu$_2$O-NPs. However, Ru-Cu$_2$O-NPs at 100 g/mL concentrations significantly reduced BM MSCs proliferation when compared to non-treated cells. Similar results were observed with HC cell lines after 24'h treatment, whereas after 48' h treatment, a significant reduction in HC proliferation was found even at
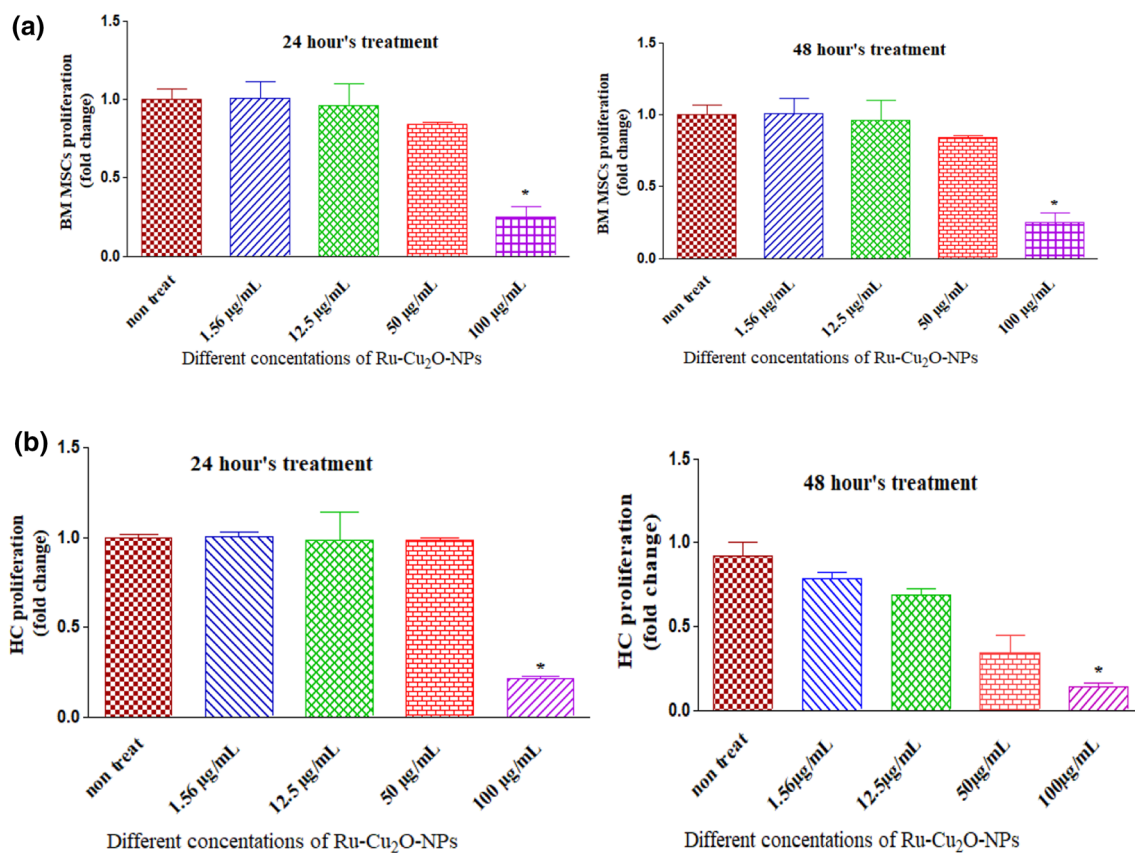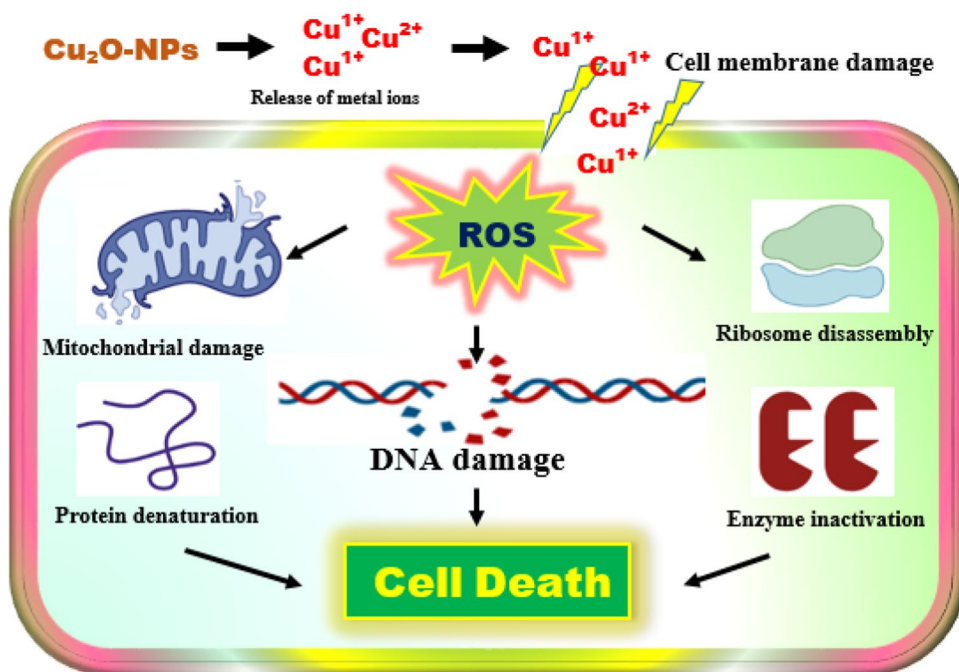
Fig. 13 Probable antimicrobial mechanism of Ru-Cu$_2$O-NPs

Fig. 14 In vitro toxicity of Ru-Cu$_2$O-NPs on BM MSCs (**a**) and HC (**b**). Superscripts [*Significant ($p < 0.05$)] showing on the bar in different concentrations

50 g/mL concentrations of Ru-Cu$_2$O-NPs. Thus, all the dose of the NP can be used as a potent vehicle for drug delivery, except the highest dose (100 μg/mL).

The CCK8 analysis results showed that both primary and metastatic colon cancer cells (SW480 and SW620) significantly ($p < 0.05$) reduced cell proliferation at treatment with 100 μg/mL concentration of Ru-Cu$_2$O-NPs. The mean difference between the control (non-treated) and 100 μg/mL dosage treatment in SW480 cells and SW620 cells was $85.1 \pm 7.14\%$ and $85.1 \pm 4.79\%$, respectively. Whereas, lower concentrations of Ru-Cu$_2$O-NPs did not have any significant effect ($p < 0.05$) on the cell proliferation of colon cancer cells as well (Figs. 15(A, B), 16).

The cytotoxic activity of nanoparticles in colon cancer cells was measured by EZBlue cell assay kit. The EZBlue cell assay results showed that the treatment with the highest dose (100 μg/mL) of nanoparticle significantly increased the cytotoxicity having the mean difference fold of 0.57 ± 0.0196 for SW480 cells and the mean difference fold of 0.427 ± 0.0174 for SW620 cells. The 50 μg/mL treatment of Ru-Cu$_2$O-NPs on SW620 cells also showed a significantly ($p < 0.05$) increased cytotoxicity of the nanoparticle having a mean difference fold of 0.206 ± 0.0159 (Fig. 15C, D). The lower concentrations do not show any significant

($p < 0.05$) cytotoxicity compared to control cells. Similarly, the 12.5 μg/mL concentration of nanoparticle treatment did not show any toxicity and morphological changes after 48'h of incubation thus can be used as potent vehicle for drug delivery. Whereas, toxicity of nanoparticles when treated in a higher dose (viz. 50 μg/mL and 100 μg/mL) on colon cancer cell lines, aided in suppressing colon cancer cell proliferation which further also supports their anticancer activities.

Khan et al. (2017) reported the less toxicity of the copper oxide nanoparticles at a concentration of 640 μg/mL. Whereas, copper nanoparticles synthesized from *Agaricus bisporus* at 500 μg/ml concentration showed cytotoxicity on SW620 cells with 60% cell viability (Sriramulu et al. 2020). Wongrakpanich et al. (2016) reported toxicity of copper oxide nanoparticles (34.9 nm) in the liver (HepG2) and intestinal cells (Caco-2 cells) at 10.90 μg/mL and 10.04 μg/mL concentrations, respectively (Wongrakpanich et al. 2016). The difference in the percent of toxicity of copper oxide nanoparticles could be due to differences in their size that affect the rate of entry of nanoparticles into the cell potentially influencing the amount of dissolution of copper ions (Wongrakpanich et al. 2016). In the present study, the toxicity was analysed after 24'h and 48'h treatments. According to Riss and Moravec (2004), Yedjou et al. (2006),

Fig. 15 Cell viability analysis of nanoparticles on primary and metastatic colon cancer cells (**A**) SW480 cells (**B**) SW620 cells and cytotoxicity effect of nanoparticles in primary and metastatic colon cancer cells (**C**) SW480 cells (**D**) SW620 cells
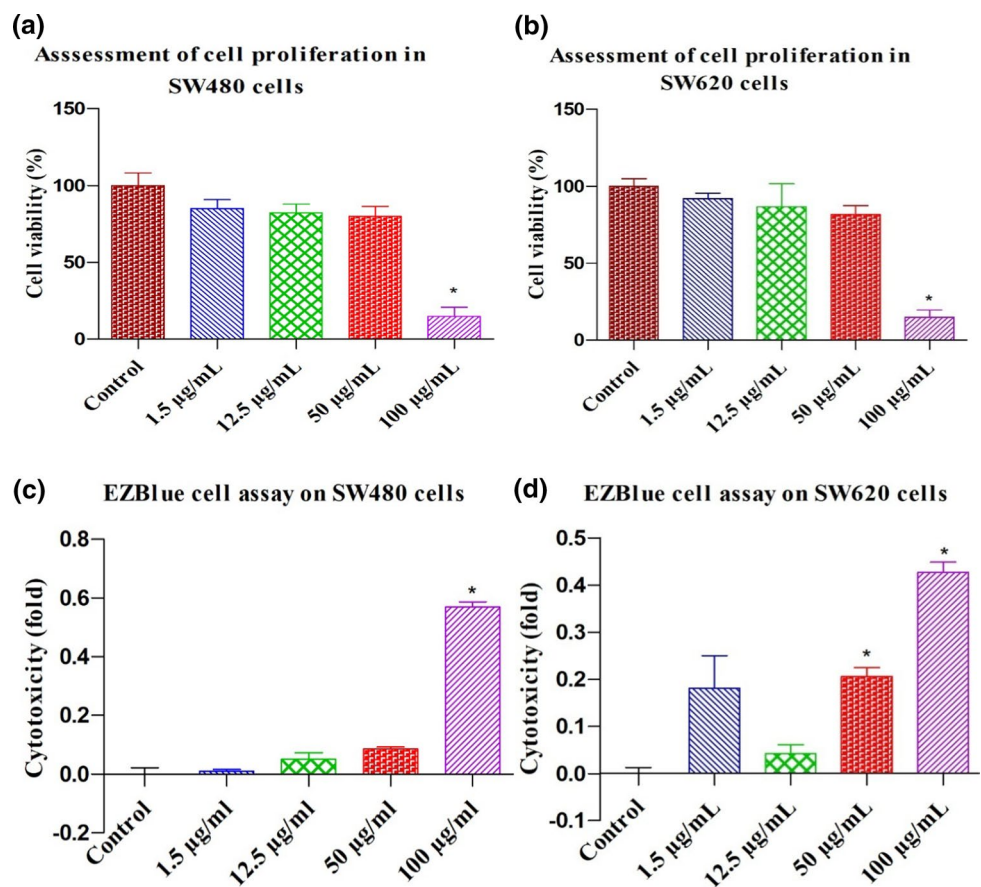
Fig. 16 Morphological analysis of primary and metastatic colon cancer cells (**A**) SW480 cells without treatment (**B**) SW480 cells treated with 12.5 µg/mL of nanoparticle (**C**) SW620 cells without treatment (**D**) SW620 cells treated with 12.5 µg/mL of nanoparticle
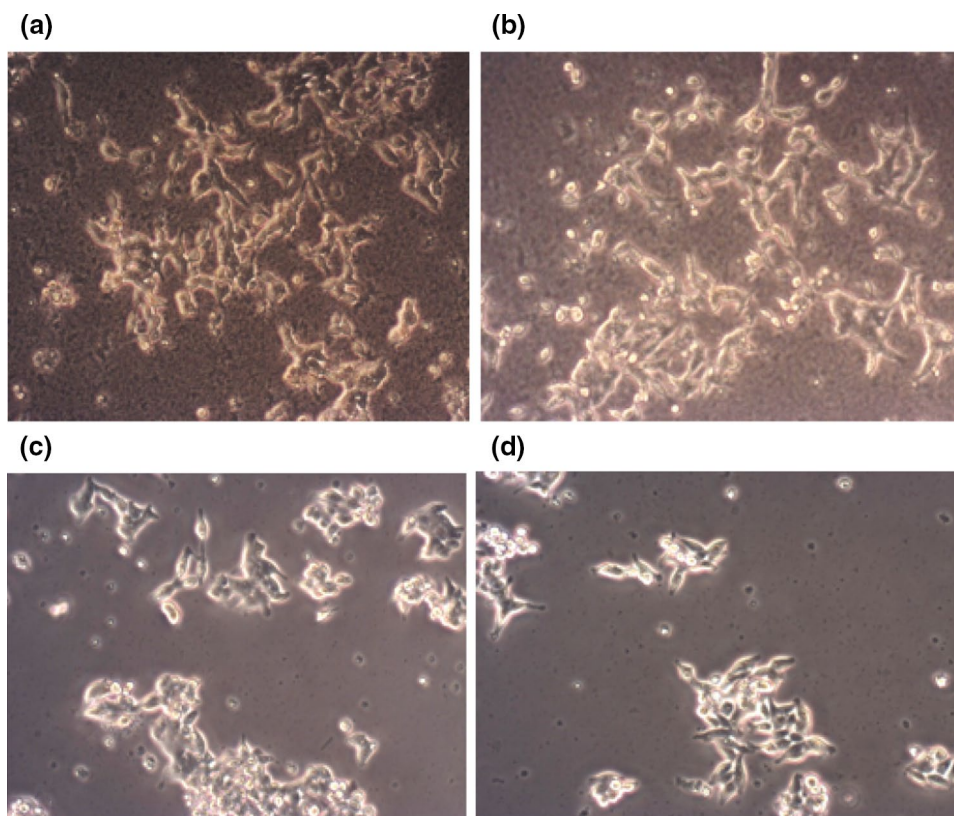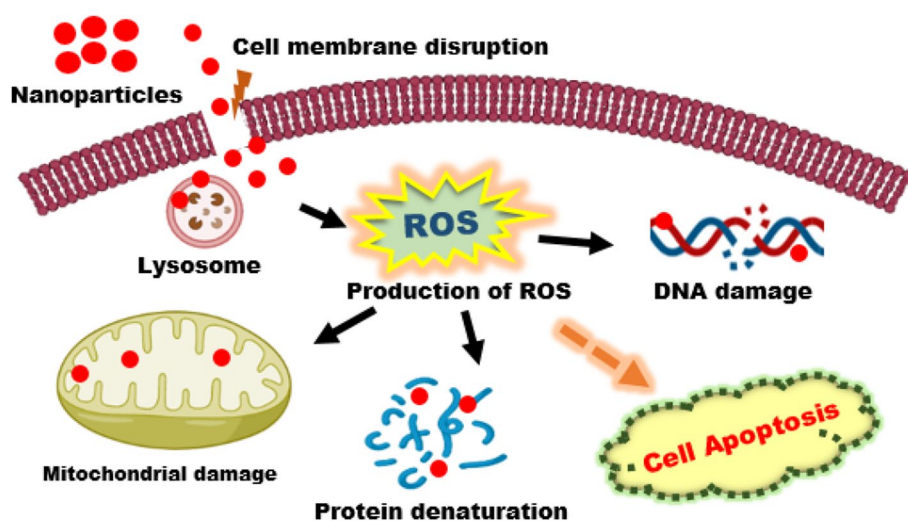

Fig. 17 Toxicity mechanism of nanoparticles

and Kang et al. (2013), the 24 h of treatment can be used for cell viability analysis and taken as the suitable period for in vitro toxicity assay. The generation of reactive oxygen species (ROS) may be induced by nanoparticle exposure, which is a major cause of toxicity. Excessive formation of reactive oxygen species (ROS) results in oxidative stress, inflammation, and consequent damage to proteins, cell membranes, and DNA, as well as cell death (Fig. 17) (Sengul and Asmatulu 2020).

Conclusion

In this study, Ru-Cu$_2$O-NPs were successfully synthesized (with an average crystallite size of 25 nm and octahedron-shaped grains with an average grain size of 0.82 ± 0.04 µm) from the aqueous fruit extract of *R. ellipticus*. Ru-Cu$_2$O-NPs showed less antioxidant activity than *R. ellipticus* fruit extract, which may be due to the presence of ascorbic acid in the fruit extract. Conversely,

Ru-Cu2O-NPs had better antimicrobial activity against *B. subtilis, S. aureus,* and *R. necatrix* than *E. coli, P. aeruginosa*, and *F. oxysporum*, making them suitable for use as antimicrobial agents. A toxicity analysis revealed that Ru-Cu$_2$O-NPs at a concentration ranging from 1.5 μg/mL, 12.5 μg/mL, and 50 μg/mL were nontoxic to BM MSCs and HC lines, supporting their use as potent drug delivery vehicles. In contrast, cytotoxicity of Ru-Cu$_2$O-NPs on colon cancer cell lines was seen at the higher doses (100 μg/mL and 50 μg/mL) which supports their anticancer properties. Moreover, the cytotoxic activity of the Ru-Cu$_2$O-NPs has zero toxicity at 12.5 μg/mL concentration, making them suitable for a variety of applications. However, further studies with clinical evaluations and in vivo techniques are needed. It is still necessary to investigate the molecular activity of NPs in animal models.

Declarations

Conflict of interest There is no conflict of interest among the authors.

References

Adinarayana TV, Mishra A, Singhal I et al (2020) Facile green synthesis of silicon nanoparticles from *Equisetum arvense* for fluorescence based detection of Fe (III) ions. Nanoscale Adv 2:4125–4532. https://doi.org/10.1039/D0NA00307G

Ahmad W, Jaiswal KK, Soni S (2020) Green synthesis of titanium dioxide (TiO$_2$) nanoparticles by using *Mentha arvensis* leaves extract and its antimicrobial properties. Inorg Nano-Met Chem 50:1032–1038. https://doi.org/10.1080/24701556.2020.1732419

Azimi H, Kuhri S, Osvet A et al (2014) Effective ligand passivation of Cu$_2$O nanoparticles through solid-state treatment with mercaptopropionic acid. J Am Chem Soc 136:7233–7236. https://doi.org/10.1021/ja502221r

Banerjee D, Chakrabarti S, Hazra AK (2008) Antioxidant activity and total phenolics of some mangroves in Sundarbans. Afr J Biotechnol 7:805–810

Bauer AW (1966) Antibiotic susceptibility testing by a standardized single disc method. Am J Clin Pathol 45:149-158

Bezza FA, Tichapondwa SM, Chirwa EM (2020) Fabrication of monodispersed copper oxide nanoparticles with potential application as antimicrobial agents. Sci Rep 10:1–18. https://doi.org/10.1038/s41598-020-73497-z

Chauhan A, Verma R, Batoo KM et al (2021) Structural and optical properties of copper oxide nanoparticles: a study of variation in structure and antibiotic activity. J Mater Res 36:1496–1509. https://doi.org/10.1557/s43578-021-00193-7

Chauhan A, Verma R, Kumari S et al (2020) Photocatalytic dye degradation and antimicrobial activities of Pure and Ag-doped ZnO using *Cannabis sativa* leaf extract. Sci Rep 10:1–16. https://doi.org/10.1038/s41598-020-64419-0

Chenthamara D, Subramaniam S, Ramakrishnan SG et al (2019) Therapeutic efficacy of nanoparticles and routes of administration. Biomater Res 23:1–29. https://doi.org/10.1186/s40824-019-0166-x

Clinical and Laboratory Standards Institute (2012) M100–S22.Performance standards for antimicrobial susceptibility testing: 22nd informational supplement. PA CLSI, Wayne

Dhatwalia J, Kumari A, Chauhan A et al (2022) *Rubus ellipticus Sm.* fruit extract mediated zinc oxide nanoparticles: a green approach for dye degradation and biomedical applications. Materials 15:3470. https://doi.org/10.3390/ma15103470

El-Saadony MT, El-Hack A, Taha ME et al (2020) Ecofriendly synthesis and insecticidal application of copper nanoparticles against the storage pest *Tribolium castaneum*. Nanomaterials 10(3):587. https://doi.org/10.3390/nano10030587

Essien ER, Atasie VN, Okeafor AO et al (2020) Biogenic synthesis of magnesium oxide nanoparticles using *Manihot esculenta* (Crantz) leaf extract. Int Nano Lett 10:43–48. https://doi.org/10.1007/s40089-019-00290-w

Fidrianny I, Rizkiya A, Ruslan K (2015) Antioxidant activities of various fruit extracts from three *solanum* sp. using DPPH and ABTS method and correlation with phenolic, flavonoid and carotenoid content. J Chem Pharm Res 7:666–672

Gebremedhn K, Kahsay MH, Aklilu M (2019) Green synthesis of CuO nanoparticles using leaf extract of *Catha edulis* and its antibacterial activity. J Pharm Pharmacol 7:327–342. https://doi.org/10.17265/2328-2150/2019.06.007

Grover R, Moore J (1962) Toximetric studies of fungicides against brown rot organisms. Sclerotinia-Fructicola s-Laxa Phytopathol 52(9):876–879

Hayashi N, Machida K, Otawara K (2018) Polymer-soluble thermostable phosphate-ester copper complexes for near-infrared absorbing dyes with weak absorbance in the visible region. Opt Mater 77:111–116. https://doi.org/10.1016/j.optmat.2018.01.020

Hussien A, Gawish SM, Mosleh SES (2019) Antimicrobial polypropylene loaded by cubic cuprous oxide micro particles. Egypt J Chem 62:1047–1055. https://doi.org/10.21608/ejchem.2019.13001.1813

Ijaz F, Shahid S, Khan SA (2017) Green synthesis of copper oxide nanoparticles using *Abutilon indicum* leaf extract: antimicrobial, antioxidant and photocatalytic dye degradation activities. Trop J Pharm Res 16:743–753. https://doi.org/10.4314/tjpr.v16i4.2

Iravani S, Korbekandi H, Mirmohammadi SV et al (2014) Synthesis of silver nanoparticles: chemical, physical and biological methods. Res Pharm Sci 9:385

Jiang P, Prendergast D, Borondics F et al (2013) Experimental and theoretical investigation of the electronic structure of Cu2O and CuO thin films on Cu (110) using X-ray photoelectron and absorption spectroscopy. J Chem Phys 138:024704. https://doi.org/10.1063/1.4773583

Kang T, Guan R, Chen X (2013) In vitro toxicity of different-sized ZnO nanoparticles in Caco-2 cells. Nanoscale Res Lett 8:1–8. https://doi.org/10.1186/1556-276X-8-496

Kasana RC, Panwar NR, Kaul RK (2016) Copper nanoparticles in agriculture: biological synthesis and antimicrobial activity. Nanoscience Food Agric 3:129–143. https://doi.org/10.1007/978-3-319-48009-1_5

Kerour A, Boudjadar S, Bourzami R (2018) Eco-friendly synthesis of cuprous oxide (Cu$_2$O) nanoparticles and improvement of their solar photocatalytic activities. J Solid State Chem 263:79–83. https://doi.org/10.1016/j.jssc.2018.04.010

Khan S, Ansari AA, Khan AA (2017) In vitro evaluation of cytotoxicity, possible alteration of apoptotic regulatory proteins and antibacterial activity of synthesized copper oxide nanoparticles. Colloids Surf B Biointerfaces 153:320–326. https://doi.org/10.1016/j.colsurfb.2017.03.005

Kumar V, Wadhwa R, Kumar N et al (2019) A comparative study of chemically synthesized and *Camellia sinensis* leaf extract-mediated silver nanoparticles. 3 biotech 9(1):1–9. https://doi.org/10.1007/s13205-018-1544-0

Kumar B, Smita K, Debut A et al (2021) Green synthesis of cuprous oxide nanoparticles using Andean Capuli (*Prunus serotina* Ehrh. var. Capuli) cherry. J Clust Sci 32:1753–1760. https://doi.org/10.1007/s10876-020-01924-2

Lal S, Verma R (2022) Chauhan A (2022) Antioxidant, antimicrobial, and photocatalytic activity of green synthesized ZnO-NPs from *Myrica esculenta* fruits extract. Inorg Chem Commun 141:109518. https://doi.org/10.1016/j.inoche.2022.109518

Lalla R, Cheek MD, Nxumalo MM (2018) First assessment of naturalised *Rubus ellipticus* Sm. populations in South Africa-A potential invasion risk? S Afr J Bot 114:111–116. https://doi.org/10.1016/j.sajb.2017.10.020

Li P, Lv W, Ai S (2016) Green and gentle synthesis of Cu₂O nanoparticles using lignin as reducing and capping reagent with antibacterial properties. J Exp Nanosci 11:18–27. https://doi.org/10.1080/17458080.2015.1015462

Mahendran G, Kumari BR (2016) Biological activities of silver nanoparticles *from Nothapodytesnimmoniana* (Graham) Mabb. fruit extracts. Food Sci Hum Wellness 5:207–218. https://doi.org/10.1016/j.fshw.2016.10.001

Maheshwaran G, Bharathi AN, Selvi MM (2020) Green synthesis of Silver oxide nanoparticles using *Zephyranthes rosea* flower extract and evaluation of biological activities. J Environ Chem Eng 8:104137. https://doi.org/10.1016/j.jece.2020.104137

Marslin G, Siram K, Maqbool Q et al (2018) Secondary metabolites in the green synthesis of metallic nanoparticles. Materials 11:940. https://doi.org/10.3390/ma11060940

Mensor LL, Menezes FS, Leitão GG et al (2001) Screening of Brazilian plant extracts for antioxidant activity by the use of DPPH free radical method. Phytother Res 15(2):127–130. https://doi.org/10.1002/ptr.687

Moller JK, Madsen HL, Aaltonen T et al (1999) Dittany (*Origanum dictamnus*) as a source of water-extractable antioxidants. Food Chem 64(2):215–219. https://doi.org/10.1016/S0308-8146(98)00143-5

Moharekar S, Raskar P, Wani A (2014) Synthesis and comparative study of zinc oxide nanoparticles with and without capping of pectin and its application. World J Pharm Pharm Sci 3(7):1255–1267

Muniyandi K, George E, Sathyanarayanan S et al (2019) Phenolics, tannins, flavonoids and anthocyanins contents influenced antioxidant and anticancer activities of *Rubus* fruits from Western Ghats, India. Food Sci Hum Well 8:73–81. https://doi.org/10.1016/j.fshw.2019.03.005

Muthukumaran M, Dhinagaran G, Venkatachalam K et al (2020) Green synthesis of cuprous oxide nanoparticles for environmental remediation and enhanced visible-light photocatalytic activity. Optik 214:164849. https://doi.org/10.1016/j.ijleo.2020.164849

Nasrollahzadeh M, Sajadi SM, Maham M (2015) Green synthesis of palladium nanoparticles using *Hippophaerhamnoides Linn* leaf extract and their catalytic activity for the Suzuki–Miyaura coupling in water. J Mol Catal A Chem 396:297–303. https://doi.org/10.1016/j.molcata.2014.10.019

Nethravathi PC, Kumar MP, Suresh D et al (2015) *Tinospora cordifolia* mediated facile green synthesis of cupric oxide nanoparticles and their photocatalytic, antioxidant and antibacterial properties. Mater Sci Semicond Process 33:81–88. https://doi.org/10.1016/j.mssp.2015.01.034

Ng CHB, Fan WY (2006) Shape evolution of Cu₂O nanostructures via kinetic and thermodynamic controlled growth. J Phys Chem B 110:20801–20807. https://doi.org/10.1021/jp061835k

Pandey Y, Bhatt SS (2016) Overview of Himalayan yellow raspberry (*Rubus ellipticus* Smith): a nutraceutical plant. J Appl Nat Sci 8:494–499. https://doi.org/10.31018/jans.v8i1.824

Pankove JI (1975) Optical Processes in Semiconductors. Courier Corporation, Massachusetts

Ramesh P, Saravanan K, Manogar P et al (2021) Green synthesis and characterization of biocompatible zinc oxide nanoparticles and evaluation of its antibacterial potential. Sens Bio-Sens Res 31:100399. https://doi.org/10.1016/j.sbsr.2021.100399

Reddy NJ, Vali DN, Rani M (2014) Evaluation of antioxidant, antibacterial and cytotoxic effects of green synthesized silver nanoparticles by *Piper longum* fruit. Mater Sci Eng C 34:115–122. https://doi.org/10.1016/j.msec.2013.08.039

Regmi A, Bhandari J, Bhattarai S et al (2019) Synthesis, Characterizations and antimicrobial activity of cuprous oxide (Cu₂O) nanoparticles. J Nepal Chem Soc 40:5–10. https://doi.org/10.3126/jncs.v40i0.27271

Rehana D, Mahendiran D, Kumar RS (2017) Evaluation of antioxidant and anticancer activity of copper oxide nanoparticles synthesized using medicinally important plant extracts. Biomed Pharmacother 89:1067–1077. https://doi.org/10.1016/j.biopha.2017.02.101

Riss TL, Moravec RA (2004) Use of multiple assay endpoints to investigate the effects of incubation time, dose of toxin, and plating density in cell-based cytotoxicity assays. Assay Drug Dev Technol 2:51–62. https://doi.org/10.1089/154065804322966315

Saini R, Dangwal K, Singh H et al (2014) Antioxidant and antiproliferative activities of phenolics isolated from fruits of Himalayan yellow raspberry (*Rubus ellipticus*). J Food Sci Technol 51:3369–3375. https://doi.org/10.1007/s13197-012-0836-3

Sannigrahi S, Mazuder UK, Pal DK et al (2010) Antioxidant potential of crude extract and different fractions of *Enhydra fluctuans* Lour. Iran J Pharma Res 9(1):75

Sengul AB, Asmatulu E (2020) Toxicity of metal and metal oxide nanoparticles: a review. Environ Chem Lett 18:1659–1683. https://doi.org/10.1007/s10311-020-01033-6

Sharma D, Thakur N, Vashistt J (2018) Antibacterial evaluation of cuprous oxide nanoparticles synthesized using leaf extract of *Callistemon viminalis*. Indian J Pharm Educ Res 52:449–455. https://doi.org/10.5530/ijper.52.3.52

Sharma R, Garg R, Kumari A (2020) A review on biogenic synthesis, applications and toxicity aspects of zinc oxide nanoparticles. EXCLI J 19:1325. https://doi.org/10.17179/excli2020-2842

Shelari PV, Katkar AS (2018) Biological synthesis of Cu₂O nanoshells and its optical properties. Int JChem Pharm Sci 7:75–80. https://doi.org/10.30731/ijcps.7.3.2018.75-80

Shende S, Gaikwad N, Bansod S (2016) Synthesis and evaluation of antimicrobial potential of copper nanoparticle against agriculturally important phytopathogens. Synthesis 1:41–47

Shirwaikar A, Shirwaikar A, Rajendran K et al (2006) In vitro antioxidant studies on the benzyl tetra isoquinoline alkaloid berberine. Biol Pharma Bull 29(9):1906–1910. https://doi.org/10.1248/bpb.29.1906

Sriramulu M, Shanmugam S, Ponnusamy VK (2020) *Agaricus bisporus* mediated biosynthesis of copper nanoparticles and its biological effects: an study. Colloid Interface Sci Commun 35:100254. https://doi.org/10.1016/j.colcom.2020.100254

Thoka S, Lee AT, Huang MH (2019) Scalable synthesis of size-tunable small Cu₂O nanocubes and octahedra for facet-dependent optical characterization and pseudomorphic conversion to Cu nanocrystals. ACS Sustain Chem Eng 7:10467–10476. https://doi.org/10.1021/acssuschemeng.9b00844

Velsankar K, RM AK, Preethi R (2020) Green synthesis of CuO nanoparticles via *Allium sativum* extract and its characterizations on antimicrobial, antioxidant, antilarvicidal activities. J Environ Chem Eng 8:104123. https://doi.org/10.1016/j.jece.2020.104123

Viet PV, Nguyen HT, Cao TM et al (2016) *Fusarium* antifungal activities of copper nanoparticles synthesized by a chemical reduction method. J Nanomater 2016:7. https://doi.org/10.1155/2016/1957612

Wang Y, Lu Y, Zhan W (2015) Synthesis of porous Cu₂O/CuO cages using Cu-based metal–organic frameworks as templates and their gas-sensing properties. J Mater Chem A 3:12796–12803. https://doi.org/10.1039/C5TA01108F

Wongrakpanich A, Mudunkotuwa IA, Geary SM et al (2016) Size-dependent cytotoxicity of copper oxide nanoparticles in lung epithelial cells. Environ Sci Nano 3:365–374. https://doi.org/10.1039/C5EN00271K

Yedjou CG, Moore P, Tchounwou PB (2006) Dose-and time-dependent response of human leukemia (HL-60) cells to arsenic trioxide treatment. Int J Environ Res Public Health 3:136–140. https://doi.org/10.3390/ijerph2006030017

Zhang X, Zhang Y, Wang D et al (2014) Investigation of adsorption behavior of Cu_2O submicro-octahedra towards congo red. J Nanomater 2014:3. https://doi.org/10.1155/2014/619239

Zhao Y, Ran W, He J et al (2015) High-performance asymmetric super-capacitors based on multilayer MnO_2/graphene oxide nanoflakes and hierarchical porous carbon with enhanced cycling stability. Small 11(11):1310–1319. https://doi.org/10.1002/smll.201401922

Zhou J, Wang C, Cunningham AJ et al (2019) Synthesis and characterization of size-controlled nano-Cu_2O deposited on alpha-zirconium phosphate with excellent antibacterial property. Mater Sci Eng C 101:499–504. https://doi.org/10.1016/j.msec.2019.04.008